*Mineralogical Magazine, February 2003, Vol. 67(1), pp. 1–13*

# Laser Raman identification of silica phases comprising microtextural components of sinters

K. A. RODGERS[1] AND W. A. HAMPTON[2,*]

[1] Research Associate, Australian Museum, College Street, Sydney, NSW, Australia
[2] Department of Geology, University of Auckland, Private Bag 92019, Auckland, New Zealand

**ABSTRACT**

Laser Raman spectroscopy is particularly well suited for routine characterization of the crystalline and the better ordered paracrystalline silica phases occurring in silica sinters: opal-C, quartz and moganite. The non-crystalline and poorly ordered paracrystalline silica phases (opal-CT and opal-A) are identified with difficulty, partly as a result of the high level of fluorescence exhibited by the younger sinters that are dominated by these phases, and partly as a result of the ill-defined nature of the broad phonon scattering bands produced by them. Nonetheless, given the limited number of phases present and the high level of phonon scattering from the better ordered phases, judicious use of a Raman microprobe enables the character of most siliceous microtextural sinter components to be determined readily. Microprobe examination of a series of New Zealand sinters, ranging from Late Quaternary to Pliocene in age shows that a silica phase inhomogeneity that exists in some outcrops reflects an underlying phase heterogeneity obtaining in the microstructure of the sinter; it is a consequence of the phase transformation process. In the older sinters, quartz, moganite and opaline cristobalite may be present in a single fabric element but in quite different proportions to their abundance in adjacent elements. Identification of opaline lepispheres partially pseudomorphed by quartz+moganite and the association of quartz+moganite in microcrystals exhibiting common quartz forms, cautions against the use of morphology as a means of identifying silica phases at the microstructural level.

**KEYWORDS:** silica, sinter, laser Raman spectroscopy, opal, New Zealand.

## Introduction

SURFACE deposits of silica sinter are a common expression of geothermal systems. They are a signature of the hydrological conditions prevailing at the time the sinter flocculated as opaline silica from near-neutral alkali chloride hot springs derived from deep reservoirs hotter than 175ºC (Fournier and Rowe, 1966). Consequently, sinters provide an important exploration guide to locating and interpreting geothermal systems whose surface activity has changed, declined or even ceased. Further, the texture of the freshly deposited opaline silica is determined, in part, by templets afforded by the microbial communities that thrive in the hot-spring environments, and hence the resulting sinters furnish invaluable information about mineral-microbe associations in hydrothermal systems (e.g. Walter *et al.*, 1996; Farmer, 2000). Sinters are a remarkable, persistent, terrestrial, sedimentary deposit.

When first deposited, silica in sinter is characteristically non-crystalline opal-A. With time the sinter crystallizes to paracrystalline opal-CT±opal-C and, subsequently, recrystallizes to microcrystalline quartz, with moganite forming as a transitory phase (Herdianita, *et al.*, 2000*a*; Rodgers and Cressey, 2001). This phase maturation is accompanied by microtextural changes. The complete transformation can take from 30,000 to 50,000 years and is parallelled by changes in the density, porosity and water content of the successive silica phases (Herdianita *et al.*, 2000*a*). The correct identification of the different

* E-mail: wendy12@clear.net.nz
DOI: 10.1180/0026461036710079

silica phases is essential to elucidating sinter history.

X-ray powder diffraction is well suited to characterizing each of the different crystalline silica minerals (Smith, 1997, 1998). Difficulties exist, however, in using conventional X-ray powder techniques to identify opal-CT, with its limited lattice order, in the presence of opal-C which possesses an enhanced but still restricted crystal structure (Smith, 1998; Herdianita *et al.,* 2000*b*; Campbell *et al.,* 2001). Further, the progression in phase transformation is not uniform within an outcrop, a fabric or textural type, or even a single hand specimen. In order to fully ascertain the stage in maturation that a sinter has attained and, importantly, to gain an understanding of the processes involved in that transformation, it is desirable to determine the phase composition of individual morphological components of different sinters. This is not possible with conventional X-ray powder techniques. The standard $20 \times 10 \times 1$ mm aluminium diffraction sample holders require 200–300 mg of powder. This is some 5–10 orders of magnitude greater than the mass of many of the sinter fabric elements. Clearly, each X-ray powder scan serves to identify only the dominant phases present in several million microtextural components. Phases present at low levels tend to be overlooked as has proved to be the case with moganite (Smith, 1998; Rodgers and Cressey, 2001). Heaney and Post (1992) found it necessary to undertake Rietveld refinement of their data after having counted for 2–10 s/0.03º2θ from 2 to 80º2θ, i.e. for 1.4–7.2 h per sample, in order to confirm the presence of moganite in microcrystalline quartz. Such requirements are not conducive for routine analyses of silica-rich samples and an alternative method to X-ray powder techniques is required if the mineralogy of individual sinter microtextures is to be determined and the interrelationships between the different silica phases comprehended at a microscopic level.

The routine identification of the principal silica species with Raman microspectroscopy has been demonstrated by Kingma and Hemley (1994) in the course of using a Raman microprobe to characterize moganite in microcrystalline quartz samples. Subsequently, Götze *et al.* (1998) employed a Raman microprobe to explore the distribution of moganite in agate while Allen *et al.* (1999) used Raman techniques successfully to characterize the agglutinated silica (and titania) particles of marine foraminifera tests. Although Herdianita *et al.* (2000*a*) and Rodgers and Cressey (2001) reported some preliminary Raman scans of opal-A, opal-CT and opal-C, the silica phases common among late Pleistocene and Recent sinters, they made no systematic study. The present report describes the results of a Raman survey of all sinter specimens used by Herdianita *et al.* along with some additional New Zealand examples, particularly from quartz-rich Tertiary deposits. These spectra are presented in their raw, unvarnished form in order to demonstrate the strengths and weaknesses of the laser Raman microprobe as a routine determinative tool in microtextural sinter studies. The results prove sufficient to demonstrate that a silica phase inhomogeneity often observed in a sinter outcrop also pertains at the microscopic level.

## Samples

Herdianita *et al.* (2000*a*) reported on 29 samples of silica sinter from ten different active and extinct geothermal systems, specifically collected to provide a range of ages and occurrences of typical thin-bedded moderate- to low-temperature sinters. Less common textural types and silica residue were excluded. Mineral phases other than silica were rare. Twenty one were from active and extinct Quaternary geothermal fields of the Taupo Volcanic Zone (TVZ). Five came from the long-lived but still active Ngawha field of northern New Zealand, and three from Tertiary occurrences in North America (Hausbrouck and Lincoln, Montana). All had been deposited from near-neutral alkali chloride waters. None had suffered subsequent heating or steam alteration as far as could be ascertained. All were examined in the present study. Specimen details are given in Herdianita *et al.* (2000*a*), although the ages of some of their samples have recently been revised.

In addition, the present study includes samples from the quartz-rich mid- to late-Pliocene Whenuaroa sinter at Plumduff and Mount Mitchell, Northland, two of three southernmost sinter masses of the fossil Puhipuhi geothermal field, as well as from late Pleistocene, >40,000 BP, sinters of Umukuri (Campbell *et al.*, 2001) and Atiamuri, from tephra-rich sinter remnants capping hillocks in the Otamakokore and Whirinaki stream valleys, and from the mid-Tertiary Waitaia Sinter of Coromandel (Skinner, 1976). Conventional X-ray powder diffraction showed all these additional specimens to contain high proportions of opaline cristobalite (opal-CT

and/or opal-C) and/or quartz. Rodgers and Cressey (2001) had demonstrated that moganite was intimately associated with microcrystalline quartz in both the lower horizons of Umukuri, quartz-rich areas of the Otamakokore erosional residuals, and some older Atiamuri sinters.

Reference samples included an unlocated, colourless, transparent quartz macrocrystal from Switzerland and tridymite from Vechec Quarry, Eastern Slovakia (AM D52115). A suitable cristobalite specimen was unavailable and the Raman spectral data given by Bates (1972) were used. Sample numbers prefixed AU are those of the University of Auckland, Department of Geology, petrology collection; that prefixed AM is from the Australian Museum mineral collection. Nomenclature of the silica phases follows Smith (1997, 1998).

## Experimental

The nature of the present exercise was to examine the variation in spectra obtained from a variety of non-crystalline, paracrystalline and crystalline microtextural components. The crystalline silica phases, quartz, α-cristobalite, α-tridymite and moganite all possess distinctive, intense scattering bands in the region 350–550 $cm^{-1}$ as do the better ordered of the paracrystalline opals (Fig. 1).

Initial experiments focused on collecting the Raman spectra of different textural portions of each sample from 150 to ~724 $cm^{-1}$, i.e. across an ~575 $cm^{-1}$ wide counting window, using a Dilor XY spectrometer of 500 mm focal length akin to that used by Kingma and Hemley (1994) and employing similar experimental procedures to those used by and Rodgers and Cressey (2001) with $Ar^{+}$ as the exciting line operating at 514.5 nm. The Raman spectra were collected at 298±3 K, using a liquid nitrogen-cooled CCD detector. Beam power was 50 mW and spectral bandpass 2.74 $cm^{-1}$, with an integration time of 120 s for the incremental window of ~600 $cm^{-1}$, with a slit of 100 $cm^{-1}$. An uncoated ×50 objective proved satisfactory for microsampling

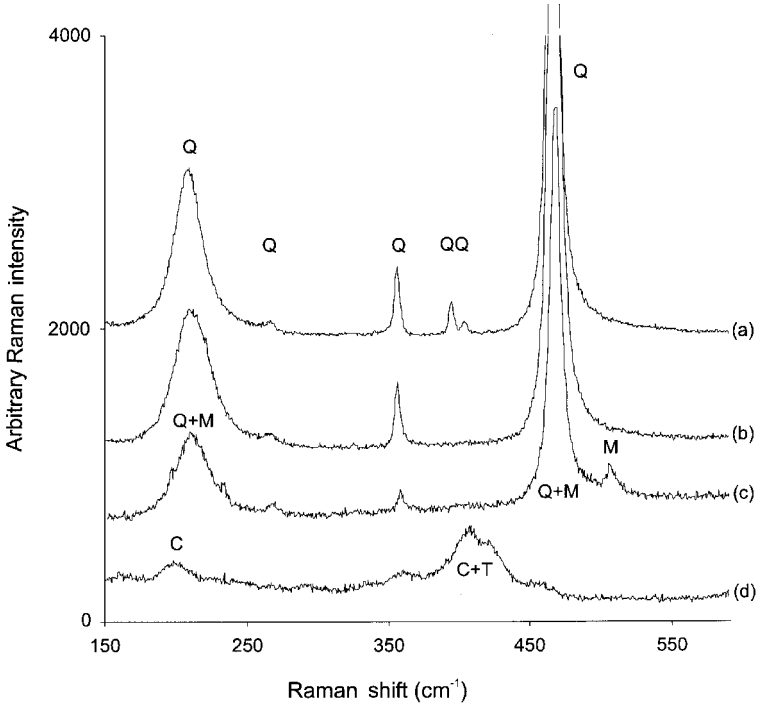


FIG. 1. Laser Raman spectral scans from 150 to 724 $cm^{-1}$ of crystalline and paracrystalline silica phases. (a,b) scans perpendicular to 100 for alternative *ac* orientations of a single quartz macrocrystal, Switzerland: (a) *c* parallel to microscopic E–W, (b) *c* parallel to microscopic N–S; (c) quartz+moganite, Umukuri sinter, AU48290; (d) tridymite with cristobalite, Vehec, AM D52115.

some of the coarser, crystalline materials but a ×100 provided a more restricted sampling area and gave less risk of counting photons scattered by fabric elements adjacent to that being examined. With a magnification of ×100, an area of ~2 μm in diameter can be sampled. While this represents a considerable improvement on conventional X-ray powder analysis it still fails to cope adequately with smaller and intergrown fabric elements that may be <1 μm. The conventional arrangement of stage and lens of the Olympus microscope gave 180º scattering geometry.

Forty samples from Whenuaroa were analysed using a Renishaw Raman 1000 system with deep depletion CCD. This permitted individual textural elements of the sinter to be recognized and targeted for mineralogical identification to an extent that was not possible with the Dilor XY. The available Raman range was 100–4000 $cm^{-1}$ using an air-cooled argon 488 nm 25 mW (blue) laser and 200–2500 $cm^{-1}$ using a solid-state 785 nm 25 mW (red) laser; the resolution was ~2 $cm^{-1}$. While the red laser proved less sensitive to fluorescence, the spectral cut-off at ~200 $cm^{-1}$ made it desirable where possible to employ the blue laser with a 25% reduction filter. A 1200 l/mm diffraction grating was used with the red laser and a 2400 l/mm with the blue. Spectra were collected with a slit of 100 μm and an integration time of 10 s under high gain. Spectral bandpass was ~2 $cm^{-1}$. The intensity of the moganite scattering bands made it desirable to collect and coadd five spectral runs from each sampled area in order to improve signal to noise ratios.

One of the advantages of the Renishaw 1000 system is to allow direct CCD imaging of the precise area of each specimen, and hence to target a specific sinter textural element (Fig. 2). Further, the quasi-confocal optics of the Renishaw model used considerably reduces the effect of stray light collection scattered from neighbouring grains such as had affected some Dilor XY results. Image resolution was ~1 μm using a ×20 objective.

In the majority of cases no preparation was undertaken beyond breaking or sawing a fresh face. The same difficulties experienced by Rodgers and Cressey (2001) were encountered when attempts were made to examine polished sinter specimens. Variable results were obtained in analysing specific textural areas of polished thin sections due to the high level of fluorescence of the particular epoxy mounting medium used. Prism faces of quartz were microsampled in a consistent orientation, where these were developed and accessible among crystals growing in cavities, allowing like spectra to be compared with like spectra. Elsewhere the size of the microcrystals and/or the massive nature of the matrix aggregates precluded consistently sampling crystals of the same orientation. A consequence of the lack of orientation is reflected in variations in the relative intensities and/or absence of some Raman bands in some spectra (e.g. Fig. 1*a,b*).

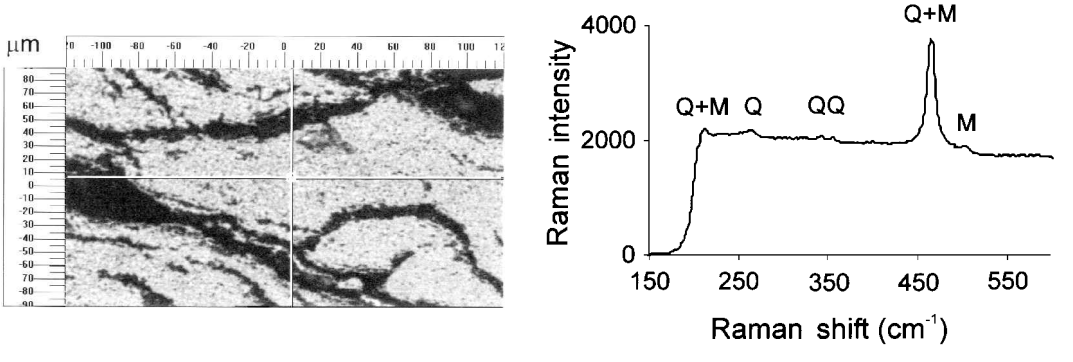


FIG. 2. Example of CCD image and raw Raman spectrum obtained from Pliocene Plumduff specimen AU53504 by the Renishaw 1000 system. Image shows an inter-fingering of blue-grey (dark) and light-brown ultrafine-grained sinter. The laser beam diameter, i.e. sampled area, is delineated by the circle at the centre of the crosshairs. Selective sampling of the two sinter types shows both to consist of quartz+moganite. Q = quartz scattering band; M = moganite scattering band.

## Results

### *Raman scattering behaviour of crystalline, paracrystalline and non-crystalline silicas*

Many of the raw Raman spectra presented here are not of high quality. In a number of respects, they represent the useful minimum of what can be obtained from a sinter using a Raman microprobe. In part, this arises from the rough surfaces, manifold imperfections, and small size of some of the textural elements microprobed. Some spectra include a high level of fluorescence that drowns the Raman signal, while the scattering behaviour of the poorly crystalline and disordered phases is akin to the limited response of these same phases to a primary X-ray beam; in both cases the scattering bands tend to be broad and ill-defined (e.g. Fig. 1). Nonetheless, the distinctive Raman scattering bands of all crystalline silica species common in sinter can be distinguished readily and the nature of all silica sinter phases present can be deduced from the results, provided these are interpreted judiciously, relying both on the negative evidence afforded by the absence of scattering bands of crystalline silica phases and the knowledge that only a limited number of silica phases is present in any sinter specimen.

A feature of the Raman spectra of the majority of younger (<10,000 BP), opal-A dominated sinters was a high level of fluorescence that effectively swamped any Raman photons. As a consequence, despite protracted quench times and/or pre-treatment of samples with 100 vol.% $H_2O_2$ to destroy any organics that may be present, no diagnostic Raman response was observed in any sinter consisting solely of opal-A. Some of this fluorescence background appears to reside in the disordered, hydrous nature of opal-A itself (Splett *et al.,* 1997).

Many older Quaternary sinters that are also predominantly opal-A have an appreciable, visible organic content e.g. Omapere (~40,000 BP). These also show high count rates that increased rapidly and uniformly with increasing wavenumber over the width of the experimental counting window of the Dilor X-Y instrument. Microprobed portions of sinters rich in opal-CT and having low but still detectable fluorescence gave a diffuse, ill-defined scattering band which mimics that seen in samples with negligible fluorescence. Occasionally, following peroxide treatment of some opal-CT-rich samples, broad (100–200 $cm^{-1}$) scattering bands centred at about 350–355 $cm^{-1}$, were observed (e.g. AU48271, Fig. 3*e*).

Those sinters rich in α-cristobalite, i.e. opal-C-bearing, show a strong band at 421±2 $cm^{-1}$ (Figs 1*d*, 3*a,d,e*, 4*a*). Cristobalite lacks the adjacent very intense band at 403 $cm^{-1}$ and the moderately intense bands at 356, 449 and 457 $cm^{-1}$ of α-tridymite (Fig. 1*d*). Where packets of tridymite are present in the silica lattice (opal-CT), these bands combine with that at 422 $cm^{-1}$ to give a broad distinctive scattering pattern in the middle of the scanned range (Fig. 3*e*). Therefore, where such a band is absent and a strong band centred at ~420 $cm^{-1}$ is detected it is concluded that opal-C constitutes the bulk of the opaline silica phase present (Fig. 3*a*).

Quartz and moganite both possess similar vibrational spectra which reflect their sharing many structural elements (Kingma and Hemley, 1994). The most intense band in quartz lies at 465 $cm^{-1}$ while that of moganite is at 501 $cm^{-1}$ (Fig. 1*c*). However, moganite also possesses a moderately intense scattering band at 463 $cm^{-1}$ and Kingma and Hemley (1994) found it necessary to use the presence (or absence) of other quartz modes such as the sharp $A_1$ vibration at 355 $cm^{-1}$ to ascertain the presence (or absence) of quartz in a sample. Rodgers and Cressey (2001) made use of the non-fundamental, broad, low-frequency, vibrational band present in the spectrum of quartz (205 $cm^{-1}$) and occurring in the moganite spectrum at a slightly higher frequency (220 $cm^{-1}$) to discriminate the two phases. This band is absent in cristobalite and tridymite. Given the spectral cut-off at 200 $cm^{-1}$, it was not possible to use this yardstick when employing the red laser on the Renishaw 1000. However, in two instances, spectra obtained by the Renishaw spectrometer showed the 377 $cm^{-1}$ scattering band of moganite.

### *Occurrence of silica phases*

As anticipated, few of the younger (<20,000 BP) sinters showed any Raman scattering bands characteristic of any crystalline or better-ordered paracrystalline silica phases that commonly occur in sinters (*cf.* Herdianita *et al.,* 2000*a*). Young (<40,000 BP) sinters are composed principally of non-crystalline opal-A and/or paracrystalline opal-CT.

Several older sinters (30-50,000 BP), identified by Herdianita *et al.* (2000*a*) and Campbell *et al.*

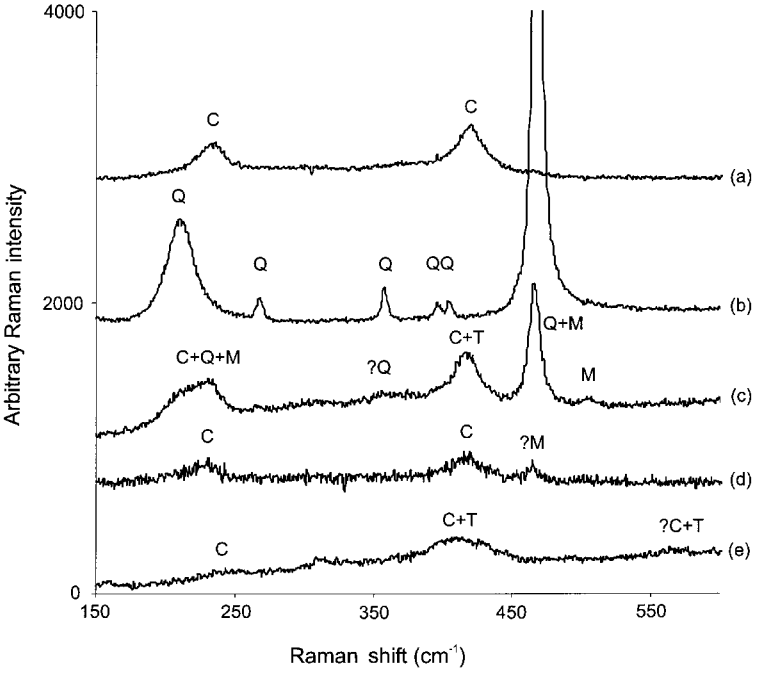


FIG. 3. Raw (unmanipulated) laser Raman microprobe spectra of late Quaternary sinters (Q = quartz; M = moganite; C = cristobalite): (a) pisoidal fabric AU48310, showing scattering broad bands of α-cristobalite; (b) monomineralic microcrystalline quartz sinter AU48290; (c) mottled palisade AU48305, showing quartz, cristobalite and moganite bands; (d) one microsampled spot of AU48310 showing bands of moganite and cristobalite and lacking a quartz band at 355 $cm^{-1}$; (e) opaline sinter, AU48271, rich in opal-CT displaying broad scattering bands centred at ~200 $cm^{-1}$ and 380 $cm^{-1}$ following peroxide treatment.

(2001) as containing appreciable opal-C, showed well defined, albeit broad bands of α-cristobalite at 418 and 230 $cm^{-1}$ (e.g. Umukuri pisoidal fabric sinter, AU48310; Fig. 3*a*). The breadth of these bands is taken as reflecting an inherently low level of long-range ordering in the opaline lattice (*cf.* Smith, 1998). It is comparable to the broadening seen in the X-ray diffraction (XRD) lines of these same samples (Herdianita *et al.*, 2000*b*).

In rare scans of some sinters rich in opal-A, a very weak quartz band at ~465 $cm^{-1}$ occurs. On the one hand this may reflect disseminated detrital quartz that is widespread, although usually at low concentration, in sinters found throughout New Zealand's Taupo Volcanic Zone, where tephra is scattered across the sinter aprons following each eruption. On the other, the signals may arise from tiny, very late-stage quartz crystals that occur infrequently in fractures in some of these young sinters. These crystals are generally not abundant enough to be discerned in routine XRD scans of most bulk samples of these sinters. They can be seen under SEM and have been detected by Raman probes of fractures (e.g. Omapere, Otamakokore). Similarly, detrital quartz can be detected in Raman-sampled spots of sinter matrix when it is present at levels insufficient to be detected in XRD scans of bulk samples.

In all sinters older than 50,000 BP, quartz is a major, if not dominant or even sole silica phase present (Fig. 3*b*). However, as reported by Rodgers and Cressey (2001), distinct moganite bands, both that at 501 $cm^{-1}$ and a skewed 210 $cm^{-1}$ broadband, occur in the spectra obtained from many quartz-dominant horizons of New Zealand sinters, particularly among those with microcrystalline quartz matrices, e.g. Umukuri AU48290, Otamakokore AU49673, Atiamuri AU47240 (Fig. 1*c*). Rodgers and Cressey (2001) failed to identify moganite in any sinter older than 200,000 BP, but in the present study moganite was found to be unevenly disseminated throughout specimens of the late

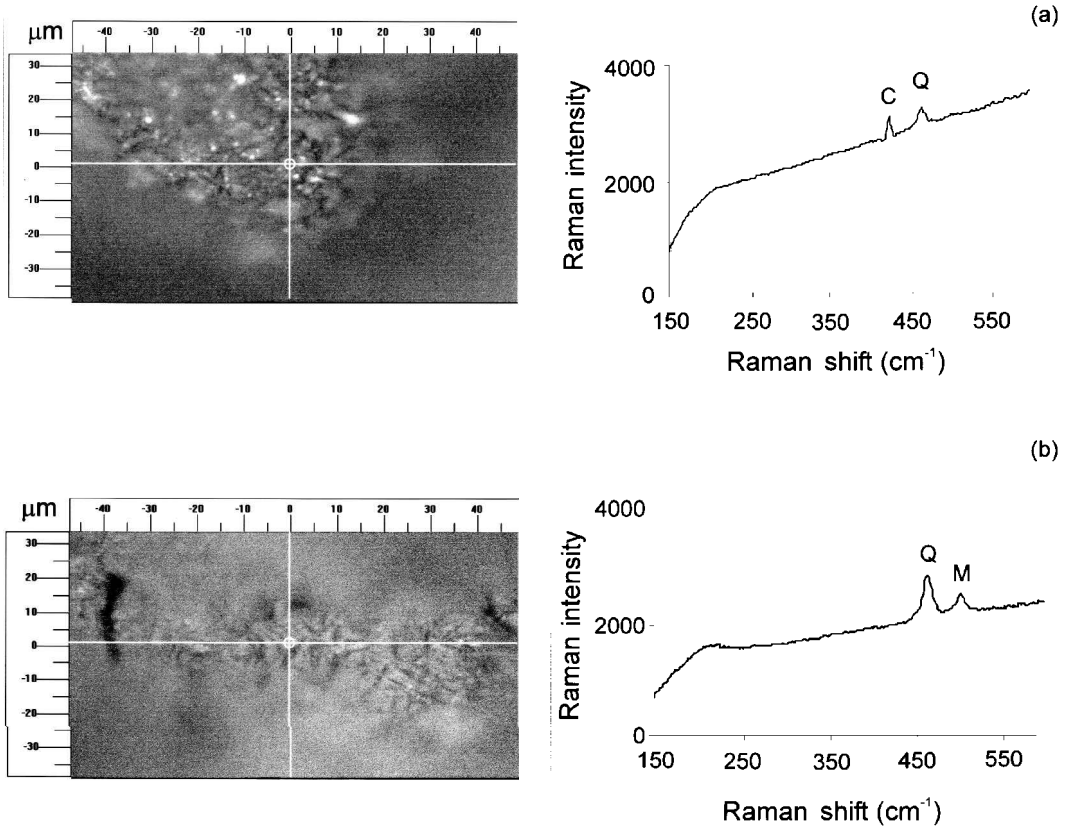


FIG. 4. CCD images and raw Raman spectra of two microsampled spots of a lepisphere in irregular fenestral sinter, AU53495, Plumduff, obtained using a Renishaw 1000 Raman microprobe system with a blue laser as the exciting line (Q,C,M as for Fig 3): (a) quartz with cristobalite; (b) quartz with significant moganite as indicated by the relative intensities of 465 and 501 $cm^{-1}$ scattering bands.

Pliocene Whenuaroa sinter outcrops at Plumduff and Mount Mitchell that otherwise consist predominantly of microcrystalline quartz. Despite the limitations outlined by Rodgers and Cressey (2001) of using Raman spectra to estimate relative proportions of different silica phases, in general the ratio of the moganite 501 $cm^{-1}$ scattering band to the composite quartz+moganite band at ~465 $cm^{-1}$ in most Whenuaroa samples is notably less than that illustrated by Rodgers and Cressey (2001) from Quaternary quartz-rich sinters of Umukuri and Otamakokore, and suggests the proportion of moganite to quartz is lower at Whenuaroa, i.e. <13%. However, in one example, AU53495 (Fig. 4*b*), the moganite 501 $cm^{-1}$ is exceptionally strong and the ratio to the composite 465 $cm^{-1}$ band 2–4 times that of the examples of Rodgers and Cressey.

The association of the scattering bands of α-cristobalite (opal-C) with quartz and moganite is not uncommon in older Quaternary sinters, e.g. in the Umukuri mottled palisade fabric AU48305 (Fig. 3*c*). In one sampled scan of AU48310 from Umukuri, moganite bands were observed together with α-cristobalite where quartz appears to be absent. Although the combined 465 $cm^{-1}$ band is quite subdued, no scattering band arising from quartz alone was observed in repeated and coadded scans, such as that at 355 $cm^{-1}$ (e.g. Fig. 3*d*). This sample proved quite inhomogeneous in respect of the distribution of its silica phases.

Rodgers and Cressey (2001) noted that, in general, moganite in the Umukuri and Otamakokore late Quaternary, quartz-rich sinters tended to be present in those smaller, bipyramidal, euhedral crystals that line sinter cavities and that

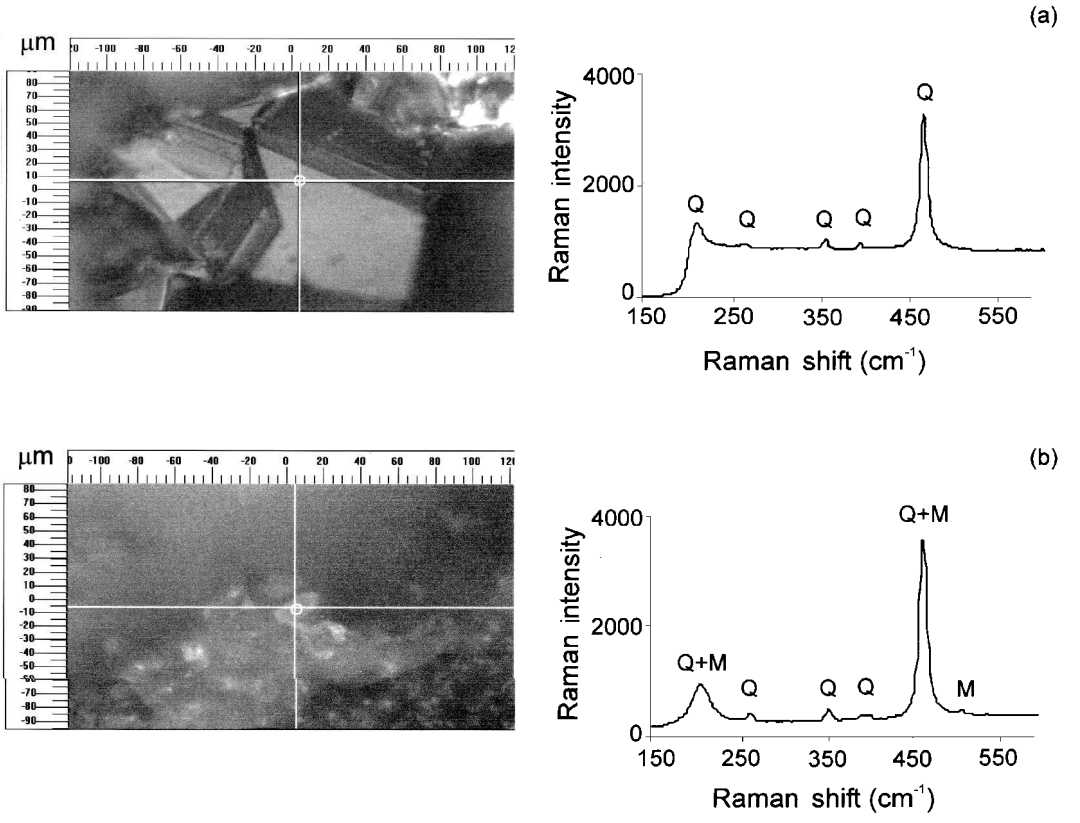


FIG. 5. CCD images and raw Raman spectra of microsampled spots of two contrasting quartz microcrystals (Q and M as for Fig. 3): (a) AU53479, late stage crystal exhibiting numerous growth striae and growing perpendicular to cavity wall and showing scattering bands of quartz alone; (b) AU3501, tiny, euhedral crystal, lacking growth striae on prism faces and developed at low angle to cavity wall, that possesses scattering bands of both quartz and moganite. The opportunities for stray light collection scattered from neighbouring grains are minimized with the confocal optics in the Renishaw Raman microprobe used to collect these spectra particularly given the size of the laser spot (circled).

form on recrystallization of opaline sinter. They failed to find definitive evidence of moganite among late-stage, fluid-deposited quartz crystals formed subsequent to the recrystallization process and which tend to be larger than those formed by recrystallization. In general, among the quartz-rich sinters of Whenuaroa, the same pattern of moganite occurrence was seen, proving it to be present among some individual quartz crystals but not others (Fig. 5*a,b*). For example, it was detected at levels estimated to be <2% in a 20 µm long crystal in AU53501 and a 10 µm crystal in AU53504, but was absent in a 180 × 120 µm crystal in AU53479 and a 40 µm crystal in AU53449. In AU53502, moganite was dispersed throughout the ultrafine-grained translucent blue-grey matrix but not present in any of cavity-lining crystals microprobed that ranged from 2 to >20 µm along *c*.

In contrast to the other silica polymorphs, β-cristobalite lacks any Raman scattering band between 300 and 700 $cm^{-1}$; its single Raman active fundamental occurs at 777 $cm^{-1}$. It was not found in any of the sinters analysed, nor would it be expected, even as a metastable phase, given its stability range. Nonetheless, Keith *et al.* (1978, p. A20) reported "β-cristobalite disordered", together with "α-cristobalite, ordered" among the older sinters of Upper Geyser Basin (*cf.* White *et al.,* 1988, in the Norris Basin). Perhaps, these identifications would be considered today as those of opal-CT and opal-C, respectively.

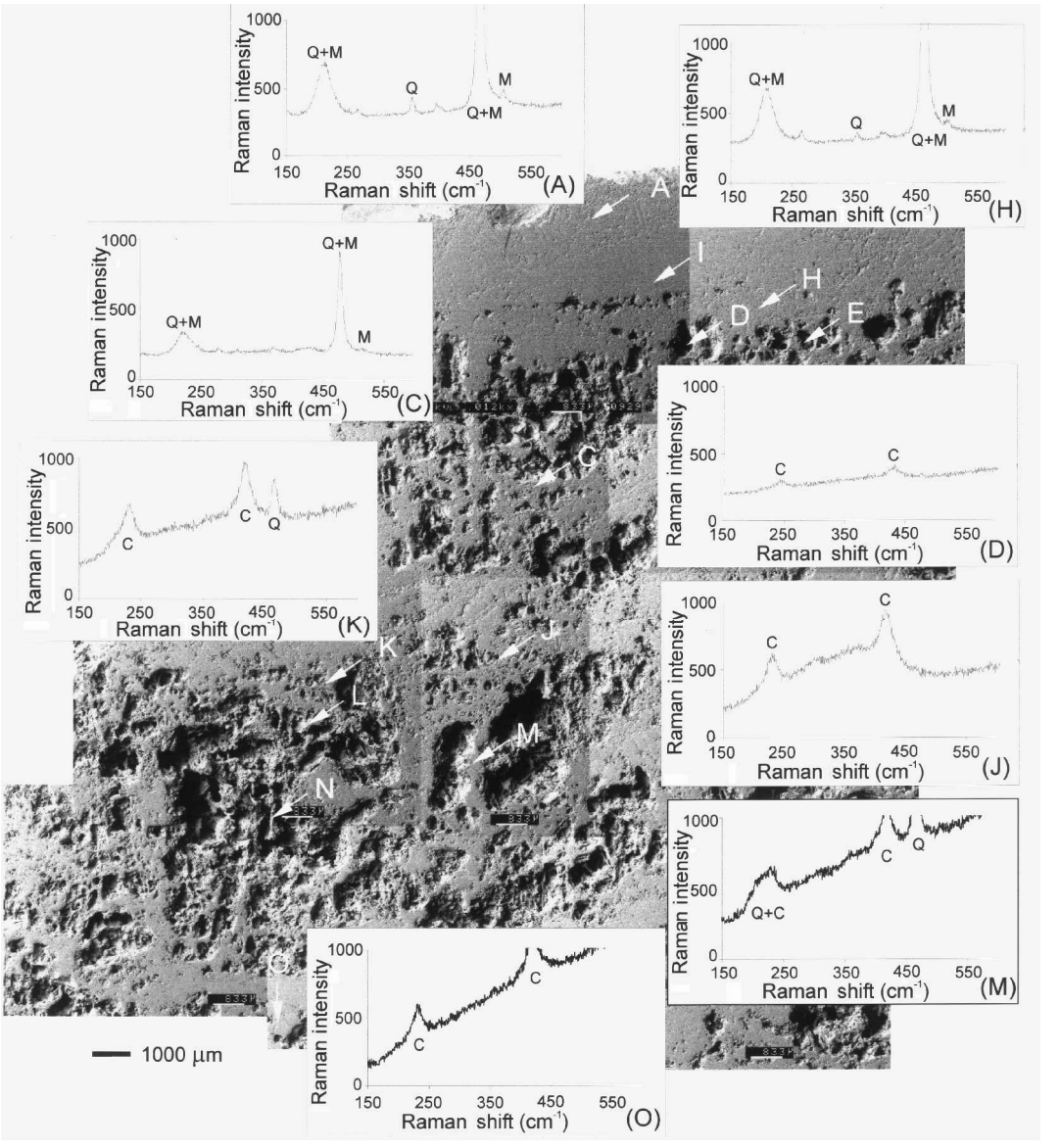


FIG. 6. Composite variable pressure SEM image of an uncoated, rough-sawn, partially crystallized slab of Umukuri opaline palisade fabric, AU48305 (*cf.* Campbell *et al.*, 2001), showing raw Raman scattering spectral results from different areas of surface (Q,M,C as for Fig. 3): (A) massive microcrystalline layer at base of slab; (C) vitreous microcrystalline matrix; (D) vitreous palisade pillar; (H) dense white microcrystalline quartz layer; (J) yellowish intercavity matrix; (K) yellowish intercavity matrix; (M) yellowish interpalisade matrix; (O) yellow weathered matrix at top of slab. The extent of the different relative intensities of the scattering bands quartz, moganite and cristobalite in the different scans are taken as evidence of inhomogeneity in the sample's surface. Note: base of sample is at top of page. Image by Chris Jones, NHM, London.

### *Textural examples*

The power and potential the Raman microprobe offers for mineralogical textural analysis of sinters finds affirmation in Fig. 6 where different textural elements of a single, rough-cut sample of mottled palisade fabric (AU48305) from Umukuri

have been microprobed (*cf.* Campbell *et al.*, 2001). In interpreting the results, allowance needs be made for the transparency of the sample and for photon scattering from areas adjacent to those being probed, but the manner in which the mineralogy of the different fabric elements can be identified is clearly evident. The microsampled areas of the specimen varied in the relative intensity (and absence) of the cristobalite, quartz and moganite scattering bands as did spectra from different sampling areas of the matrix of some specimens in which only quartz and moganite were present, e.g. Atiamuri AU47240 (Fig. 7).

A similar pattern of microscopic inhomogeneity is evident in the considerably older, quartz-rich, heavily recrystallized and mineralized Whenuaroa sinter. Importantly, it is not a pattern made manifest by conventional X-ray powder analysis. The Raman microprobe failed to detect any moganite scattering in any recrystallized examples of primary sinter palisade, tufted network or finely-laminated facies. It was, however, recognized in portions of blue-grey matrix and in clasts of both fenestral network and columnar fabric types, although it was not uniformly distributed in any of these. For example, in an example of irregular fenestral sinter, AU53495, moganite was discerned in a solid band of vitreous silica transecting the sample but not in the corroded, porous matrix surrounding this band. Similarly, it was detected in one vitreous white clot in recrystallized columnar sinter AU53481 but was absent in a seemingly identical clot ~4 mm distant. Varicoloured, translucent, vitreous, chalcedonic clasts in sinter breccias proved both moganite-bearing and moganite-free as, indeed, was the matrix of some breccias. For example, blue-grey clasts of ultrafine-grained sinter in AU53501 and AU53472 contained moganite but it was absent from the texturally similar, albeit light-brown, matrix of these same rocks. In contrast, AU53504 moganite was present in both blue-grey clasts and light-brown matrix.

In the case of the Otamakokore massive mottled sinter, AU49673, the Raman results demonstrate that the specimen is bimineralic and

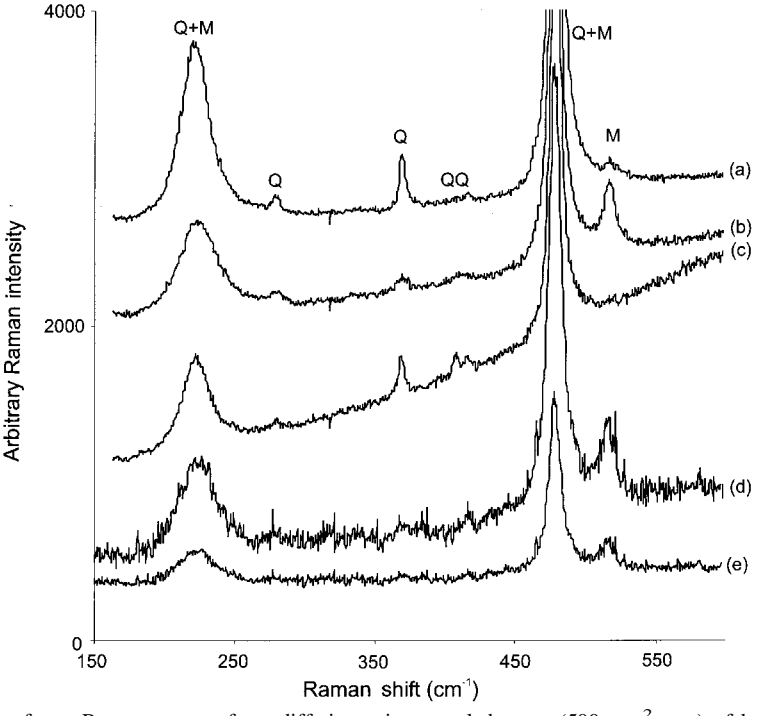


FIG. 7. Examples of raw Raman spectra from differing microsampled spots (500 $mm^2$ area) of broken surface of recrystallized, quartz-rich sinter from Atiamuri, AU47240 (Q,M as for Fig. 3). The variation in the relative intensities of the principal scattering bands of quartz and moganite in the different spectra are taken as evidence of inhomogeneity in the sample's surface.

more or less homogeneous (Fig. 8), in contrast to Atiamuri sinter AU47240 (Fig. 7). Not only do the spectra of three dozen spots in a 100 $mm^2$ area of AU49673 display the same scattering bands but the relative intensities of the quartz to moganite bands are more or less similar, regardless of the area probed. Paradoxically, in this instance the transparent nature of the sample and the opportunities for Raman scattering from areas adjacent to those being probed provide support for deducing a uniformity of sample.

The irregular fenestrae sinter sample from Plumduff, AU53495, that proved high in moganite contains abundant microbotryoidal masses of lepispheres, <50 μm in diameter. The Raman spectra obtained from the lepispheric plates by targeted Renishaw sampling using a long focal length ×50 objective, contains, along with the scattering bands of moganite and quartz, those of cristobalite (Fig. 4*a,b*). This is the oldest sinter from New Zealand in which cristobalite has been identified and it is notable that the characteristic X-ray powder patterns of opal-CT or opal-C were not observed in >90 traces obtained from a wide textural range of Whenuaroa sinter specimens.

## Discussion

A principal advantage of the Raman microprobe as a determinative tool for sinters lies in its ability to microsample individual textural elements. Coupled with the high rate of spectral acquisition available from the latest generation of instruments, the limited sample preparation, and the ability to directly target individual domains, the technique allows the twin paths of phase and textural maturation of sinters to be mapped simultaneously, at least in their later stages of development. This contrasts with techniques such as conventional powder diffraction that allow for identification of only bulk, albeit small (~400 mg), samples that can not always be clearly related to specific microtextural components. Certainly, in sinter specimens containing opal-A, and to a lesser extent opal-CT, Raman does not allow the full range of silica phases present to be unambiguously identified, nor for the degree of lattice order and disorder of the different silica phases to be evaluated. On the other hand, in those samples lacking strong fluorescence, the absence of scattering bands of

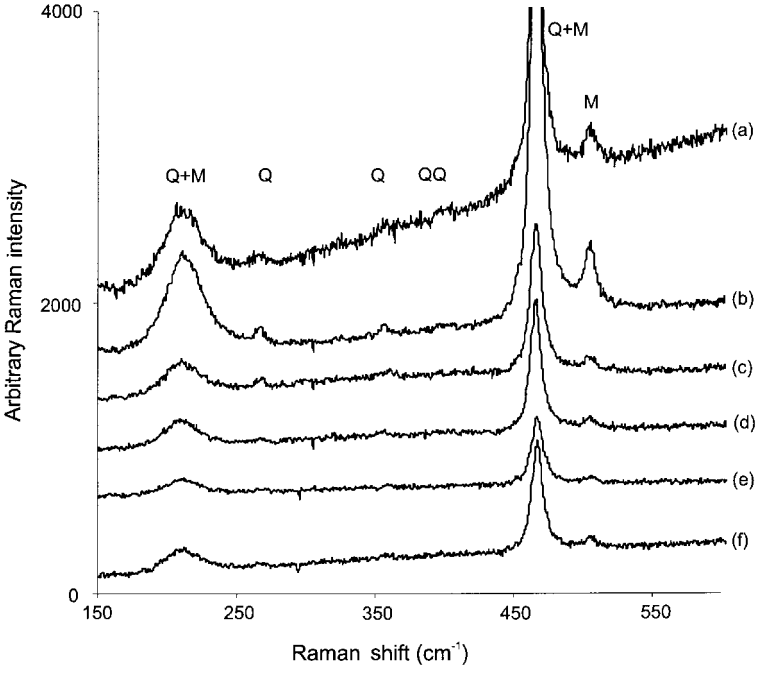


FIG. 8. Examples of raw Raman spectra from a series of 30 different microsampled spots within a 100 $mm^2$ area of Otamakokore massive mottled sinter, AU49673. (Q and M as for Fig. 3). The similarities in the relative intensities of the principal scattering bands of quartz and moganite in the different scans are taken as evidence of relative homogeneity in this portion of the specimen's surface.

well crystallized phases can be taken as indicating not only the absence of these phases but also, presumably, the presence of poorly crystalline or non-crystalline silicas – given the limited number of silica phases present in sinters.

Of particular importance is the manner in which the Raman microprobe frees the sinter worker from the need to rely on morphology as a means of identifying silica phases at the ultrastructural level. Indeed, the present results caution against relying on phase morphology as a primary determinative tool. The habit of the Plumduff quartz+moganite+opal-C lepispheres closely matches examples typical of opal-CT morphologies described by Campbell *et al.* (2001, Fig. 6*b* and *d*) from the Umukuri sinter, and from elsewhere in the Taupo Volcanic Zone (Rodgers, 2000, 2001). The Plumduff examples are presumably partially pseudomorphous after opal-CT. The implications this mixed assemblage holds for morphological-based identifications of silica phases are also contained in the dual mineralogy of the moganite+quartz crystals that exhibit typical quartz forms. Such implications are significant when determining the onset and hence timing of phase changes in sinters.

Perhaps the most significant result of both the present study and that of Rodgers and Cressey (2001) is confirmation that the silica phase inhomogeneity exists at microstructural level. Campbell *et al.* (2001) described outcrops at Umukuri that consist of intergrown, irregular patchy masses of quartz-rich and opal-C-rich sinter. Given the surficial conditions under which sinters undergo their transformation, the slight differences between these conditions and those that existed during a sinter's original deposition, and the largely solid-state nature of the metamorphosis, clear-cut, dramatic boundaries between phases and textures are not to be expected. However, the present results demonstrate that such macroscopic inhomogeneity merely reflects an underlying inhomogeneity pertaining at the microstructural level.

The result is in keeping with Landmesser's (1995) innovative diffusion model for silica transport and accumulation in sedimentary environments and which, among other matters, would facilitate the transformation process. As a result of the extreme sluggishness of the silica phase transformation processes at ambient temperatures, a direct consequence of Landmesser's model is that a heterogeneity of product will be expected to obtain throughout much of the transformation process – exactly what is seen in the Raman evidence. However, the extent of inhomogeneity in the samples analysed here and the relatively very small size of the Raman sampled areas are such, that many thousands of measurements would need to be made before any distribution pattern of silica phases might be deduced that had real meaning at the outcrop, let alone in individual hand specimens.

## Acknowledgements

This study is a contribution to the Auckland Sinter Programme. It was undertaken in part with the assistance of the award to KAR of a Visiting Fellowship by the University of Technology, Sydney, and of a Senior Bursary by the Mineralogical Society. The Williams family and GRD Macraes Ltd generously allowed access to Plumduff and Mount Mitchell. Funds were contributed to WAH from an AusIMM Education Endowment Trust Scholarship, a Society of Economic Geologists Foundation-BHP Student Research Grant, from the Geothermal Institute Freeston Licensing Trust and a University of Auckland Centennial Award. We thank Professor Evan Leitch (UTS, Sydney), Drs Pat Browne and John Seakins (Auckland), Drs Allan Ball, Gordon Cressey and Chris Jones (Natural History Museum, London), and Ross Pogson (Australian Museum, Sydney) for assistance and/or fruitful discussions. Louise Cotterall assisted with the figures.

## References

Allen, K., Roberts, S. and Murray, J.W. (1999) Marginal marine agglutinated foraminifera; affinities for mineral phases. *Journal of Micropalaeontology*, **18**, 183–191.

Bates, J.B. (1972) Raman spectra of α and β cristobalite. *Journal of Chemical Physics*, **57**, 4042–4047.

Campbell, K.A., Sannazzaro, K., Rodgers, K.A., Herdianita, N.R. and Browne, P.R.L. (2001) Sedimentary facies and mineralogy of the Late Pleistocene Umukuri silica sinter, Taupo Volcanic Zone, New Zealand. *Journal of Sedimentary Research*, **71**, 727–746.

Farmer, J.D. (2000) Hydrothermal systems: doorways to early biosphere evolution. *GSA Today*, **10**, 1–9.

Fournier, R.O. and Rowe, J.J. (1966) Estimation of underground temperatures from the silica content of water from hot springs and wet-steam wells. *American Journal of Science*, **264**, 685–697.

Götze, J., Nasdala, L., Kleeberg, R. and Wenzel, M. (1998) Occurrence and distribution of "moganite" in agate/chalcedony: a combined micro-Raman, Rietveld and cathodoluminescence study. *Contributions to Mineralogy and Petrology*, **133**, 96–105.

Heaney, P.J. and Post, J.E. (1992) The widespread distribution of a novel silica polymorph in microcrystalline quartz varieties. *Science*, **255**, 441–443.

Herdianita, N.R., Browne, P.R.L., Rodgers, K.A. and Campbell, K.A. (2000*a*) Mineralogical and morphological changes accompanying aging of siliceous sinter and silica residue. *Mineralium Deposita*, **35**, 48–62

Herdianita, N.R., Rodgers, K.A. and Browne, P.R.L. (2000*b*) Routine procedures to characterise the mineralogy of modern and ancient silica sinter deposits. *Geothermics*, **29**, 65–81.

Keith, T.E.C., White, D.E. and Beeson, M.H. (1978) Hydrothermal alteration and self-sealing in Y-7 and Y-8 drill holes in the northern part of Upper Geyser Basin, Yellowstone National Park, Wyoming. *United States Geological Survey Professional Paper*, **1054–A**, 26 pp.

Kingma, K.J. and Hemley, R.J. (1994) Raman spectroscopic study of microcrystalline silica. *American Mineralogist*, **79**, 269–273.

Landmesser, M. (1995) Mobilität durch Metastabilität: $SiO_2$ Transport und Akkumulation beiniedrigen Temperaturen. *Chemie der Erde*, **55**, 149–176.

Rodgers, K.A. (2000) Research on silica sinters. *Mineralogical Society Bulletin* 126(April), 16–17.

Rodgers, K.A. (2001) Silica phases of New Zealand sinters. Geodiversity Symposium, Australian Museum, 4 December 2001. *Journal and Proceedings of the Royal Society of New South Wales*, **134**, 112–113.

Rodgers, K.A. and Cressey, G. (2001) The occurrence, detection and significance of moganite ($SiO_2$) among some silica sinters. *Mineralogical Magazine*, **65**, 157–167.

Skinner, D.N.B. (1976) Sheet N40 and parts of Sheets N35, N36 and N39 Northern Coromandel (1st edition). *Geological Map of New Zealand 1:63,360.* Map (1 sheet) and notes (28 p.) New Zealand Department of Scientific and Industrial Research, Wellington, New Zealand.

Smith, D.K. (1997) Evaluation of the detectability and quantification of respirable crystalline silica by X-ray powder diffraction. *Powder Diffraction*, **12**, 200–227.

Smith, D.K. (1998) Opal, cristobalite, and tridymite: noncrystallinity versus crystallinity, nomenclature of the silica minerals and bibliography. *Powder Diffraction*, **13**, 2–19.

Splett, A., Splett, Ch. and Pilz, W. (1997) Dynamics of the Raman background decay. *Journal of Raman Spectroscopy*, **28**, 481–485.

Walter, M.R., Des Marais, D., Farmer, J.D. and Hinman, N.W. (1996) Lithofacies and biofacies of Mid-Paleozoic thermal spring deposits in the Drummond Basin, Queensland, Australia. *Palios*, **11**, 497–518.

White, D.E., Hutchinson, R.A. and Keith, T.E.C. (1988) The geology and remarkable thermal activity of Norris Geyser Basin, Yellowstone National Park, Wyoming. *US Geological Survey Professional Paper*, **1456**, 1–84.

[*Manuscript received 3 May 2002: revised 7 August 2002*]